# Hyperstructured Illumination

Evgenii Narimanov*

School of Electrical and Computer Engineering and Birck Nanotechnology Center, Purdue University, West Lafayette, Indiana 47906, United States

ABSTRACT: We present a new approach to super-resolution optical imaging, based on structured illumination in hyperbolic media. The proposed system allows for planar geometry, has unlimited field of view, and is robust with respect to optical noise and material losses.

KEYWORDS: *super-resolution, structured illumination, metamaterials, hyperbolic metamaterials*
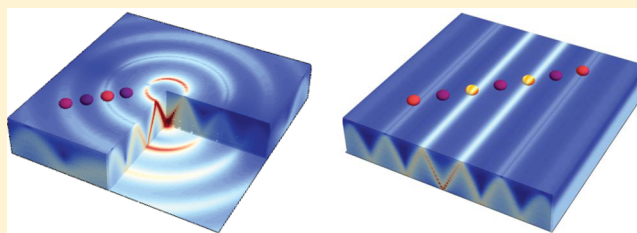
Fueled primarily by the promise[1] of optical imaging beyond the diffraction limit, metamaterials,[2] artificial composites with the unit cell size well below the optical wavelength, now for more than a decade remain one of the primary foci of modern research. However, while metamaterial devices, from the originally promised superlens[1] based on the negative index media to its younger challenger the hyperlens[3,4] that uses hyperbolic metamaterials, have been demonstrated in experiment[5,6] in a broad range of frequencies and even extended to other wave phenomena such as ultrasound imaging,[7] they have yet to find their way to broad acceptance in real-world applications.

The inherent curvature of the metamaterial device that is necessary for optical magnification (either in the general form factor of the device[3,4,8] or in its unit cell topology[9]), leading to the requirement of precise positioning of the object at subwavelength scale, remains a major practical obstacle to a wider acceptance of metamaterial-based imaging systems. More important, however, is the result of substantial loss in metamaterial structures, which is generally a direct and inevitable consequence of using metallic (or other negative permittivity) components that remain necessary for either the negative-index metamaterials or hyperbolic media. Faced with an order of magnitude intensity loss[5] as the cost of producing a magnified optical image of a subwavelength pattern, one must either accept a prohibitive cost in the signal-to-noise ratio or substantially increase the intensity of the field that illuminates the target. The latter option however does not fit well with the constraints of biomedical imaging, where high optical fields may severely damage biological tissue.

While directly related to the fundamental restrictions on optical metamaterials[10] via the Kramers−Kronig relations, this problem however allows a natural and straightforward solution: the metamaterial component of a super-resolution imaging setup must be located "in front", rather that "after", the object, so that it is probed by the already attenuated field, thus avoiding damage. This is precisely the case in the structured illumination[11] approach to optical imaging, where a grid pattern, usually generated through the interference of incident light, is superimposed on the specimen.[11,12] The imaging resolution is then determined by the periodicity of the illuminating field, and for illumination from free space this limit reduces to one-quarter of the wavelength, $\Delta = \lambda_0/4$. However, as we demonstrate in the present paper, hyperbolic metamaterials that are free from the conventional diffraction limit and can support optical patterns with the periodicity that is orders of magnitude below the free-space wavelength, λ_0, can dramatically improve the imaging resolution in structured illumination. The resulting *hyperstructured illumination* approach to super-resolution imaging is the main objective of this work.

■ STRUCTURED ILLUMINATION IN HYPERBOLIC MEDIA

In a conventional transparent medium with the refractive index n, the frequency ω generally limits the magnitude of the wavenumber k to the value of $n\omega/c$. However, the situation is dramatically different in the world of hyperbolic metamaterials,[3] where the opposite signs of the dielectric permittivity components in two orthogonal directions ($\epsilon_\tau \epsilon_n < 0$; see the inset in Figure 1a) lead to a hyperbolic dispersion of p-polarized propagating waves:
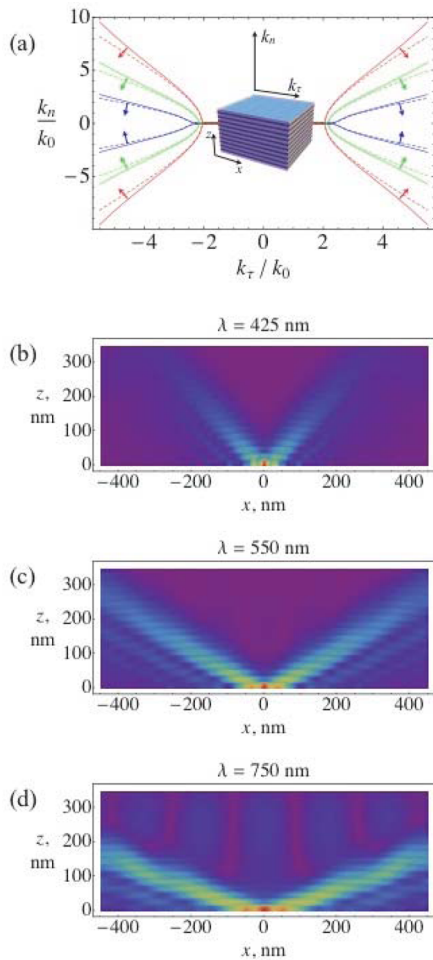
$$\frac{k_\tau^2}{\epsilon_n} + \frac{k_n^2}{\epsilon_\tau} = \frac{\omega^2}{c^2} \tag{1}$$

with the wave numbers unlimited by the frequency. For $k \gg \omega/c$, the hyperbolic isofrequency surface of eq 1 asymptotically approaches a cone, with $k_n \simeq \sqrt{-\frac{\epsilon_\tau}{\epsilon_n}} k_\tau$

As the direction of the group velocity $\mathbf{v}_g$ corresponding to a given wavevector $\mathbf{k}$ coincides with the normal to the isofrequency surface, at large wavenumbers in a uniaxial

Figure 1. (a) Isofrequency curves in a silver-glass hyperbolic metamaterial, for three different free-space wavelengths λ_0: 425 nm (blue curves), 550 nm (green), and 750 nm (red). Solid curves are obtained from the exact calculation taking into account the finite width ($a = 5$ nm) and the actual material loss of each layer, while the dashed lines correspond to the effective medium approximation (see eq 1). The arrows normal to the isofrequency curves indicate the directions of the group velocity. The inset shows the schematics of the silver-glass hyperbolic metamaterial and introduces the coordinate system. (b−d) Magnetic field intensity for light of different wavelengths ($\lambda_0 = 425$ nm (b), 550 nm (c), and 750 nm (d)), incident from $z < 0$ half-space onto the hyperbolic metamaterial formed on top of a thick silver film with a narrow slit centered at $x = 0$. The slit is parallel to the y-axis and is 5 nm wide in the x-direction. Note the conical emission pattern typical for any point source in a hyperbolic medium and strong sensitivity of its directionality to the wavelength.

hyperbolic medium the angle between the group velocity and the material symmetry axis $\hat{z} \equiv \hat{n}$ (see the inset to Figure 1a) approaches the value of $\theta_c = \arctan\sqrt{-\epsilon_\tau/\epsilon_n}$. As a result, for a point source placed at the edge of such a medium, the emission intensity diagram forms a conical pattern (see Figure 1b−d, calculated for a practical realization of hyperbolic media using a silver-glass layered metamaterial), with the "thickness" of the expanding conical "sheet" of electromagnetic radiation well below the free-space wavelength. This phenomenon is now well established[13] and has recently been successfully used for subwavelength optical lithography.[14]

As strong material dispersion is inherent to hyperbolic materials, a change in the frequency ω will result in a substantial

variation of the emission cone angle θ_c, as illustrated in Figure 1a for three different wavelengths. While generally considered detrimental to metamaterial applications (since this would immediately push the system away from whatever resonant condition it was designed for), it is precisely this property that is essential to the concept of the hyperstructured illumination. While a single source (or an opening) at the bottom of the hyperbolic "substrate" illuminates only a small part of the object plane at its "top", a change in the electromagnetic frequency would allow sweeping the entire object plane (see Figure 1b− d). As a result, a complete subwavelength image can be obtained in a single hyperspectral measurement.

This behavior is further illustrated in Figure 2, which shows the object formed by four silicon nanowires on top of the silver-
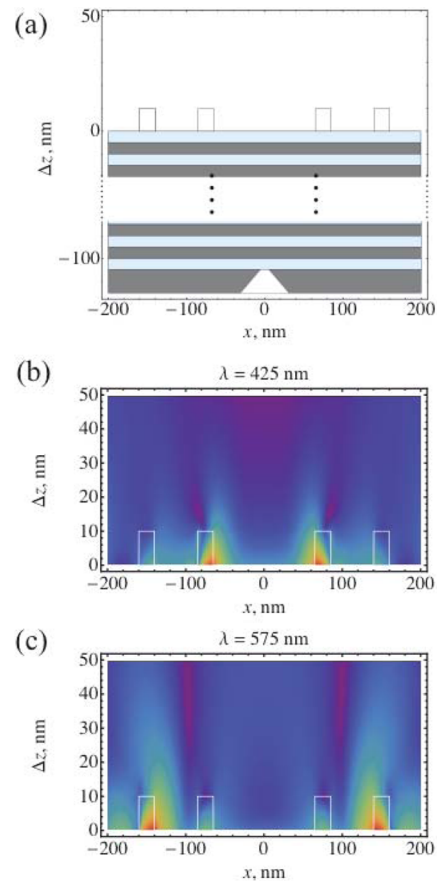
Figure 2. Hyperstructured illumination, with silver-glass hyperbolic metamaterial substrate. (a) Geometry of the imaging system, with dark and light gray regions corresponding to silver and glass layers (each 5 nm thick), respectively. Depending on the illumination wavelength, light incident from the slit at the bottom of the metamaterial illuminates different areas of the target; see panels (b) and (c), with a subdiffraction resolution. The imaging target consists of four long silicon nanowires with a rectangular cross-section of 20 nm × 10 nm, aligned along the y-direction. The false-color representation shows the magnitude of the magnetic field, calculated taking full account of the material absorption in the system.

glass metamaterial (10 silver and 11 glass layers, each 5 nm thick; see Figure 2a), illuminated at wavelengths of 425 nm (panel b) and 575 nm (panel c). Note the subwavelength localization of the electromagnetic field near the object and a dramatic difference in the intensity distribution for different

wavelengths, which allows to clearly resolve distinct elements of the target despite their close spacing.

A finite size of the unit cell of the metamaterial, a, introduces an upper limit on the (Bloch) wavenumber, $k_n \equiv k_z$, equal to $k_n^{max} = \pi/a$, as well as quantitative corrections to the dispersion $\omega(\mathbf{k})$ and to the geometry of the isofrequency surface, leading to its deviations from the hyperbolic shape. However, the overall topology of the isofrequency surface, together with its dependence on the wavelength, is generally preserved; see Figure 1a. As a result, one will still observe the general profile of the conical illumination pattern, as well as its evolution with the wavelength, that is consistent with the predictions of the effective medium theory, as clearly seen in Figure 1b−d. However, as the size of the unit cell limits the maximum wavenumber that can be supported by the propagating waves in the hyperbolic metamaterial, it defines the ultimate resolution limit Δ of the hyperstructured illumination:

$$\Delta \simeq a \qquad (2)$$

With the scale of the unit cell in high-quality hyperbolic metamaterials that have already been demonstrated, on the order of a few nanometers,[15] eq 2 allows for optical imaging of deeply subwavelength objects, to the point of resolving large individual molecules.

■ DEPTH OF FIELD IN HYPERSTRUCTURED ILLUMINATION AND THE MOTTI PROJECTION

While a hyperbolic metamaterial supports propagating electromagnetic waves with the characteristic length scale up to its unit cell size, these waves will evanescently decay outside. this medium. As a result, the imaging resolution of the proposed hyperstructured illumination setup will rapidly deteriorate with Δz (see Figure 2a), approaching the diffraction-limited value of $\lambda_0/4$ for $\Delta z \gg \lambda_0$. For a 3D object structured at a deeply subwavelength scale, the proposed imaging system based on hyperstructure illumination will resolve the Motti projection[16] $\Delta_M\epsilon(x, y)$ of its three-dimensional permittivity distribution $\epsilon(\mathbf{r})$:
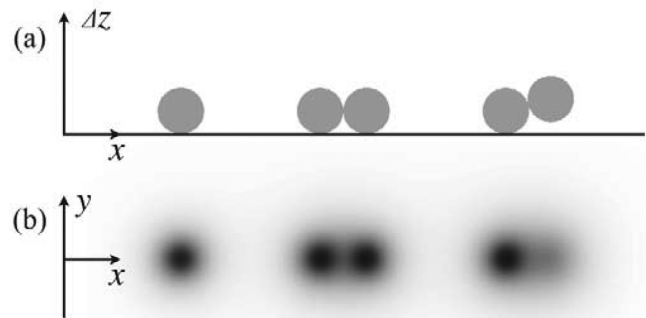
$$\Delta_M\epsilon(x, y) = \int \frac{d^3\mathbf{r}'(z'/2\pi)(\epsilon(\mathbf{r}') - 1)}{((x - x')^2 + (y - y')^2 + z'^2)^{3/2}} \qquad (3)$$

Note that the integral transformation in eq 3 is independent of the illumination wavelength and does not introduce an additional length scale: the effective averaging in eq 3 is defined by the distance z' to the object plane. As a result, eq 3 reduces the resulting resolution Δ to the corresponding depth of fields Δz. This is illustrated in Figure 3, which shows the Motti projection (panel b) for several solid spheres near the object plane $\Delta z = 0$.

■ THEORETICAL FRAMEWORK

When illuminated from the holes at the "bottom" of the hyperbolic substrate (see Figure 2a), an object with the dielectric permittivity $\epsilon(\mathbf{r})$ placed near the image plane $\Delta z = 0$ will induce scattered light with the far-field amplitudes for the s and p polarizations:

$$E_s(\mathbf{k}; \omega) = \frac{4\pi^2\omega^2}{c^2 k_n k_\tau}\{(\mathbf{p_k} \cdot [\hat{n} \times \mathbf{k}])$$

$$+ r_s(\mathbf{k}')(\mathbf{p_k} \cdot [\hat{n} \times \mathbf{k}'])\} \qquad (4)$$

Figure 3. Group of five identical solid spheres positioned near the object plane (a) and their Motti projection (b), shown in gray scale. Note the reduced contribution to $\Delta_M\epsilon(x, y)$ at longer separation from the object plane $\Delta z = 0$.

$$E_p(\mathbf{k}; \omega) = \frac{4\pi^2\omega}{c k_n k_\tau}\{([\mathbf{p_k} \times \mathbf{k}] \cdot [\hat{n} \times \mathbf{k}])$$

$$- r_p(\mathbf{k}')([\mathbf{p_{k'}} \times \mathbf{k}'] \cdot [\hat{n} \times \mathbf{k}'])\} \qquad (5)$$

where k_τ and k_n correspond to the tangential and normal to the surface of the hyperbolic substrate components of the far-field wavevector $\mathbf{k} \equiv (\mathbf{k}_\tau, \mathbf{k}_n)$, $\hat{n}$ is the normal to the surface unitary vector, r_s and r_p are the reflection coefficients at the air−substrate interface for the s- and p-polarizations, $\mathbf{k}' \equiv (\mathbf{k}_\tau, -\mathbf{k}_n)$, and $\mathbf{p_k}$ is the spatial Fourier transform of the polarization of the object, $\mathbf{p}(\mathbf{r}) \equiv (1/4\pi)(\epsilon(\mathbf{r}) - 1)E_i(\mathbf{r}, \omega)$, when it is illuminated by the incident field $E_i(\mathbf{r}, \omega)$. For an object placed close to the image plane and with the vertical dimension well below the free-space wavelength ($\Delta z \ll \lambda_0$), the polarization of the object $\mathbf{p_k}$ can be related to the spatial Fourier transform $\Delta_M\epsilon(\mathbf{q})$ of its Motti projection (eq 3):

$$\mathbf{p_k} = \frac{1}{8\pi^2} \int d^2\mathbf{q} E_i(\mathbf{k} + \mathbf{q}; \omega)\Delta_M\epsilon(\mathbf{q}) \qquad (6)$$

Given the hyperspectral measurement of the far-field $E(\mathbf{k}, \omega)$, the system of coupled linear equations (eqs 4, 5) can be used to calculate $\Delta_M\epsilon$. In particular, when the hyperstructured illumination pattern $E_i(x, y)$ at the image plane $\Delta z = 0$ originates from a periodic array of holes in a metal layer at the bottom of the substrate, separated by the distances of d_x and d_y in the x and y directions,

$$E_i(x, y; \omega) = \sum_{m_x=-\infty}^{\infty} \sum_{m_y=-\infty}^{\infty} E_0(x - m_x d_x, y - m_y d_y; \omega) \qquad (7)$$

then each spatial Fourier component of the object profile $\Delta\epsilon(\mathbf{q})$ is coupled only to a discrete set of other spatial components, which are different by an integer multiple of the reciprocal lattice vectors $(2\pi/d_x)\hat{x}$ and $(2\pi/d_y)\hat{y}$:

$$\sum_{n_x, n_y=-\infty}^{\infty} G_{n_x, n_y}^{(s,p)}(\mathbf{k}; \omega)\delta\epsilon_{n_x, n_y} = \frac{2c k_n k_\tau}{\omega} E_{(s,p)}(\mathbf{k}; \omega) \qquad (8)$$

where $\delta\epsilon_{n_x n_y} \equiv \Delta_M\epsilon[\mathbf{k}_\tau + \hat{x}(2\pi n_x/d_x) + \hat{y}(2\pi n_y/d_y)]$, and

$$G_{n_x, n_y}^{(s)}(\mathbf{k}; \omega) = (1 + r_s)([\hat{n} \times \mathbf{k}] \cdot \mathbf{e}_{n_x, n_y}(\omega)),$$

$$G_{n_x, n_y}^{(s)}(\mathbf{k}; \omega) = \frac{c}{\omega}([\hat{n} \times \mathbf{k}] \cdot [\mathbf{e}_{n_x, n_y}(\omega) \times (\mathbf{k} - r_p\mathbf{k}')]),$$
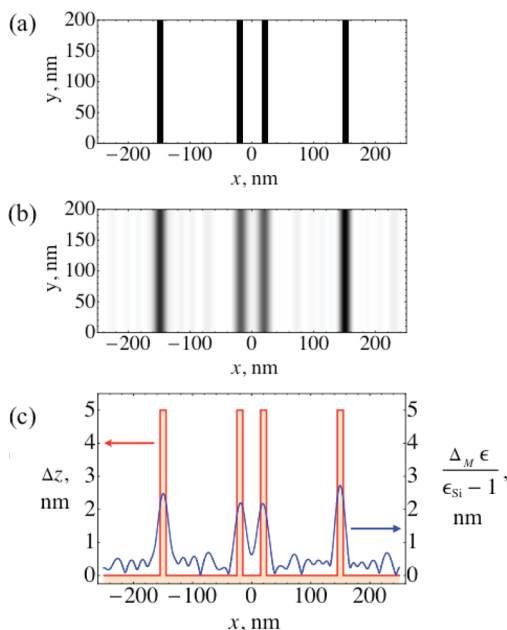
with

$$\mathbf{e}_{n_x, n_y}(\omega) \equiv \frac{1}{d_x d_y} \int d^2\mathbf{r} \mathbf{E}_0(\mathbf{r};\, \omega) e^{2\pi i (x n_x / d_x + y n_y / d_y)}$$

Given the desired resolution Δ, this implies a summation by $n_{max} \approx d/\Delta$ terms in either direction. Even with $\Delta \approx 10$ nm and diffraction-limited hole-to-hole spacing $d \approx \lambda_0/2$, we find $n_{max} \approx 100$, thus reducing the numerical complexity of solving eq 8 to that of inverting a 100×100 matrix. On a modern CPU, such a computational task can be completed within a 0.1 ms time frame. Thus, despite the need for data postprocessing that is inherent to structured illumination methods, the proposed approach can be successfully used for real-time imaging of the dynamical processes at sub-millisecond time scales.

■ HYPERSTRUCTURED ILLUMINATION IN A NOISY ENVIRONMENT

The linear inversion procedure of the previous section is robust to the presence of the noise and material absorption, which is illustrated in Figure 4, where panels (a) and (b) present the

Figure 4. Super-resolution imaging with hyperstructured illumination. (a) "Top view" of the object (four identical silicon nanowires with 10 × 5 nm cross-section) on the silver-glass hyperbolic substrate (see Figure 2a). (b) Reconstructed image, in gray scale. The calculation includes the effects of the actual material loss in the silver-glass hyperbolic substrate. (c) Object profile (red) and the (normalized to the silicon permittivity ϵ_{Si}) reconstructed Motti projection $\Delta_M \epsilon /(\epsilon_{Si} - 1)$ (blue).

gray-scale projection of the original object and its image obtained in a noisy environment. For a quantitative comparison, panel (c) shows the dimensions of the original object (left scale) and the recovered Motti projection (right scale). Note that the 30 nm separation, which is less than 1/10 of the shortest illumination wavelength, is clearly resolved, despite a substantial amount of noise in the system.

Note that the theoretical framework of the previous section is not limited to the case of an effectively one-dimensional target such as the one considered in Figure 4, but describes the general case of an arbitrary spatial dependence of the dielectric

permittivity of the object $\epsilon(\mathbf{r})$ (see eqs 3 and 6). In general this would not substantially increase the numerical complexity of solving eq 8 as long as the corresponding matrix G is not poorly defined. The can be avoided if the ratio of the periods d_y/d_x is *not* close to any of the (finite) sets of rational numbers m/n, with both of the integers m and n below the ratio of the absorption length in the hyperbolic metamaterial to its thickness.

The hyperstructured illumination approach can also be extended to the case of a *random* distribution of the illumination holes at the bottom of the hyperbolic metamaterial substrate. This would, however, substantially increase the numerical complexity of solving the equivalent of eq 3, as it would transform into an integral, rather than algebraic, system of equations.

Finally, material defects and layer-to-layer variations in the hyperbolic metamaterial substrate would simply reduce the coherence of the illumination field while preserving its general subwavelength intensity structure. The resulting incoherent hyperstructured illumination approach, while reducing the amount of information that can be determined on the composition and geometry of the target, would offer substantial advantages in a practical implementation (such as reduced noise sensitivity).

■ DISCUSSON AND CONCLUSIONS

The hyperstructured illumination approach introduced in the present paper combines deeply subwavelength resolution with the relative simplicity of *planar* geometry, which would facilitate surface functionalization for cell targeting and imaging, essential for biomedical applications. Compared to the existing super-resolving extensions of structured illumination, such as the plasmonic structured illumination,[17] the proposed approach is not limited to particular resonant wavelength (such as the surface plasmon wavelength) and is not sensitive to the material absorption.

In terms of the actual fabrication of the required metamaterial substrate, it is well within the limits of already demonstrated capabilities,[15] and experimental demonstration of the proposed imaging method will be straightforward.

■ AUTHOR INFORMATION

Corresponding Author
*E-mail: evgenii@purdue.edu.

Notes
The authors declare no competing financial interest.

■ ACKNOWLEDGMENTS

■ REFERENCES

(1) Pendry, J. B. Negative Refraction Makes a Perfect Lens. *Phys. Rev. Lett.* **2000**, *85*, 3966−3969.

(2) Cai, W.; Shalaev, V. M. *Optical Metamaterials*; Springer, 2010.

(3) Jacob, Z.; Alekseyev, L. V.; Narimanov, E. Optical Hyperlens: Far-field imaging beyond the diffraction limit. *Opt. Express* **2006**, *14*, 8247−8256.

(4) Salandrino, A.; Engheta, N. Far-field subdiffraction optical microscopy using metamaterial crystals: Theory and simulations. *Phys. Rev. B: Condens. Matter Mater. Phys.* **2006**, *74*, 075103-1−075103-5.

(5) Liu, Z.; Lee, h.; Xiong, Y.; Sun, C.; Zhang, X. Far-field optical hyperlens magnifying sub-diffraction-limited objects. *Science* **2007**, *315*, 1686.

(6) Smolyaninov, I. I.; Hung, Y. J.; Davis, C. C. Magnifying superlens in the visible frequency range. *Science* **2007**, *315*, 1699−1701.

(7) Li, J.; Fok, L.; Yin, X.; Bartal, G.; Zhang, X. Experimental demonstration of an acoustic magnifying hyperlens. *Nat. Mater.* **2009**, *8*, 931−934.

(8) Pendry, J. B. Perfect cylindrical lenses. *Opt. Express* **2003**, *11*, 755−760.

(9) Wang, W.; Xing, H.; Fang, L.; Liu, Y.; Ma, J.; Lin, L.; Wang, C.; Luo, X. Far-field imaging device: planar hyperlens with magnification using multi-layer metamaterial. *Opt. Express* **2008**, *16*, 21142−2114810.1364/OE.16.021142.

(10) Stockman, M. I. Criterion for Negative Refraction with Low Optical Losses from a Fundamental Principle of Causality. *Phys. Rev. Lett.* **2007**, *98*, 177404−1−177404−4.

(11) Gustafsson, M. G. Surpassing the lateral resolution limit by a factor of two using structured illumination microscopy. *J. Microsc.* **2000**, *198*, 82−87.

(12) Gustafsson, M. G.; Shao, L.; Carlton, P. M.; Wang, C. J. R.; Golubovskaya, I. N.; Cande, W. Z.; Agard, D. A.; Sedat, J. W. Three-Dimensional Resolution Doubling in Wide-Field Fluorescence Microscopy by Structured Illumination. *Biophys. J.* **2008**, *94*, 4957−4970.

(13) Thongrattanasiri, S.; Podolskiy, V. A. Hyper - gratings: nanophotonics in planar anisotropic metamaterials. *Opt. Lett.* **2009**, *34*, 890−892.

(14) Ishii, S.; Kildishev, A. V.; Narimanov, E.; Shalaev, V. M.; Drachev, V. P. Sub-wavelength interference pattern from volume plasmon polaritons in a hyperbolic medium. *Laser Photonics Rev.* **2013**, *7*, 265−271.

(15) Shen, H.; Lu, D.; VanSaders, B.; Kan, J. J.; Xu, H.; Fullerton, E.; Liu, Z. Anomalously Weak Scattering in Metal-Semiconductor Multilayer Hyperbolic Metamaterials. *Phys. Rev. X* **2015**, *5*, 021021-1−021021-9.

(16) Morse, P. M.; Feshbah, H. *Methods of Theoretical Physics*; McGraw-Hill, 1953.

(17) Wei, F.; Liu, Z. Plasmonic structured illumination microscopy. *Nano Lett.* **2010**, *10*, 2531−2536.